Published in final edited form as:
Clin Cancer Res. 2009 July 15; 15(14): 4712–4721. doi:10.1158/1078-0432.CCR-08-2635.

Imaging biomarkers to predict response to anti-HER2 (ErbB2) therapy in preclinical models of breast cancer

Chirayu Shah[*,1,2], **Todd W. Miller**[*,3], **Shelby K. Wyatt**[*,1,2], **Eliot T. McKinley**[1,4], **Maria Graciela Olivares**[5], **Violeta Sanchez**[3], **Donald D. Nolting**[1], **Jason R. Buck**[1,2], **Ping Zhao**[1], **M. Sib Ansari**[1,2], **Ronald M. Baldwin**[1,2], **John C. Gore**[1,2,4,5,6,7,8,9], **Rachel Schiff**[13,14,15], **Carlos L. Arteaga**[3,7,10,11], and **H. Charles Manning**[1,2,4,7,8,11,12]

[1]Vanderbilt University Institute of Imaging Science (VUIIS), Vanderbilt University Medical Center, Nashville, TN, 37232.

[2]Department of Radiology and Radiological Sciences, Vanderbilt University Medical Center, Nashville, TN, 37232.

[3]Department of Medicine, Vanderbilt University Medical Center, Nashville, TN, 37232.

[4]Department of Biomedical Engineering, Vanderbilt University Medical Center, Nashville, TN, 37232.

[5]Department of Pathology, Vanderbilt University Medical Center, Nashville, TN, 37232.

[6]Department of Physics and Astronomy, Vanderbilt University Medical Center, Nashville, TN, 37232.

[7]Vanderbilt-Ingram Comprehensive Cancer Center, Vanderbilt University Medical Center, Nashville, TN, 37232.

[8]Program in Chemical and Physical Biology, Vanderbilt University Medical Center, Nashville, TN, 37232.

[9]Department of Molecular Physiology and Biophysics, Vanderbilt University Medical Center, Nashville, TN, 37232.

[10]Department of Cancer Biology, Vanderbilt University Medical Center, Nashville, TN, 37232.

[11]Breast Cancer Research Program, Vanderbilt University Medical Center, Nashville, TN, 37232.

[12]Department of Neurosurgery, Vanderbilt University Medical Center, Nashville, TN, 37232.

[13]Dan L. Duncan Cancer Center, Baylor College of Medicine, Houston, Texas, 77030.

[14]Lester and Sue Smith Breast Center, Baylor College of Medicine, Houston, Texas, 77030.

[15]Department of Medicine, Baylor College of Medicine, Houston, Texas, 77030.

Abstract

Purpose—To evaluate non-invasive imaging methods as predictive biomarkers of response to trastuzumab in mouse models of HER2-overexpressing breast cancer. The correlation between tumor regression and molecular imaging of apoptosis, glucose metabolism, and cellular proliferation was evaluated longitudinally in responding and non-responding tumor-bearing cohorts.

Corresponding author: H. C. Manning, Vanderbilt University Institute of Imaging Science (VUIIS), 1161 21st Ave. S., AA 1105 MCN, Nashville, TN, 37232, henry.c.manning@vanderbilt.edu.
*These authors contributed equally to this work.

Experimental Design—Mammary tumors from MMTV/HER2 transgenic female mice were transplanted into syngeneic female mice. BT474 human breast carcinoma cell line xenografts were grown in athymic nude mice. Tumor cell apoptosis (NIR700-Annexin-V accumulation), glucose metabolism ([^{18}F]FDG-PET), and proliferation ([^{18}F]FLT-PET) were evaluated throughout a bi-weekly trastuzumab regimen. Imaging metrics were validated by direct measurement of tumor size and immunohistochemical (IHC) analysis of cleaved caspase-3, phosphorylated AKT (p-AKT) and Ki67.

Results—NIR700-Annexin-V accumulated significantly in trastuzumab-treated MMTV/HER2 and BT474 tumors that ultimately regressed, but not in non-responding or vehicle-treated tumors. Uptake of [^{18}F]FDG was not affected by trastuzumab treatment in MMTV/HER2 or BT474 tumors. [^{18}F]FLT PET imaging predicted trastuzumab response in BT474 tumors but not in MMTV/HER2 tumors, which exhibited modest uptake of [^{18}F]FLT. Close agreement was observed between imaging metrics and IHC analysis.

Conclusions—Molecular imaging of apoptosis accurately predicts trastuzumab-induced regression of HER2(+) tumors and may warrant clinical exploration to predict early response to neoadjuvant trastuzumab. Trastuzumab does not appear to alter glucose metabolism substantially enough to afford [^{18}F]FDG-PET significant predictive value in this setting. Although promising in one preclinical model, further studies are required to determine the overall value of [^{18}F]FLT-PET as a biomarker of response to trastuzumab in HER2+ breast cancer.

Keywords

Annexin-V; [^{18}F]FDG-PET; [^{18}F]FLT-PET; trastuzumab; HER2; breast cancer; treatment response; apoptosis; imaging

INTRODUCTION

The American Cancer Society estimates that 178,480 women were diagnosed with breast cancer in the U.S. in 2007 (1). Twenty to thirty percent of breast cancers exhibit amplification or overexpression of the HER2/erbB2 oncogene, which is associated with more aggressive disease and poor prognosis (2,3). HER2 is a member of the epidermal growth factor receptor (EGFR) family of tyrosine kinases, which includes HER1/erbB1 (EGFR), HER2/erbB2, HER3/erbB3, and HER4/erbB4. These receptors regulate a wide range of cellular processes including proliferation, differentiation, motility, survival, angiogenesis, invasion and anti-apoptotic functions (4). To date, an endogenous ligand for the HER2 receptor has not been identified, but its activation is thought to occur through heterodimerization with other ligand-bound HER family members or by homodimerization when highly expressed (4).

The development of inhibitors targeting various portions of the HER signaling axis is an active and clinically important area of research. Trastuzumab (Tz, Herceptin®) is an FDA-approved, recombinant, humanized monoclonal antibody that selectively binds to the extracellular domain of HER2 (5). In combination with chemotherapy, Tz extends overall survival and slows disease progression in HER2+ breast cancer patients. However, approximately 50% of HER2 + metastatic breast cancers exhibit *de novo* or acquired resistance to Tz (6–9) and objective means to assess early response to Tz therapy remain undeveloped.

Although the primary mechanism(s) of action of Tz remains unclear (10), the importance of phosphatidylinositol-3 kinase (PI3K) signaling in HER2+ breast cancer (4) implies that perturbation of this pathway is important in order for HER2-directed therapies to exert an anti-tumor effect. This also implies that PI3K-regulated processes such as tumor cell apoptosis, proliferation, and glucose metabolism may be useful biomarkers of response to Tz therapy. Indeed, a recent study in patients with HER2+ breast cancer showed that after one week of

neoadjuvant treatment with Tz as a single agent, a significant increase in tumor cell apoptosis was observed by cleaved caspase-3 immunostaining of tumor sections from core biopsies (11). HER2 signaling activates the PI3K/AKT/mTOR cascade and activated AKT stimulates the transport and metabolism of glucose (12). It has been shown that genes encoding most glycolytic enzymes are under dominant transcriptional control by AKT and TOR activities (13). Since Tz inhibits PI3K activation in HER2+ breast cancer cells (14), glucose metabolism may be altered by Tz therapy. Similarly, one might also predict that tumor cell proliferation would be inhibited by Tz therapy, yet in a recent study the proliferation marker Ki67 did not change in HER2+ tumors from patients treated with Tz (11). While these and other *ex vivo* assays are potentially valuable, procurement of tumor tissues through biopsies for the assessment of drug action is invasive and limited by sample bias stemming from tumor heterogeneity and other confounding factors such as inflammation. Serial biopsy, as would be required to assess the effects of therapy, is also clinically impractical in many cases. Alternatively, non-invasive molecular imaging biomarkers, which are capable of serial assessment of numerous relevant biological processes, could be particularly valuable towards clinical evaluation and prediction of response to Tz in patients with HER2+ breast cancer.

In these preclinical investigations, we sought to evaluate and validate three noninvasive molecular imaging metrics as biomarkers of response to Tz in two clinically relevant mouse models of HER2+ breast cancer. The imaging metrics evaluated include assessment of apoptosis with an optical imaging analogue of Annexin-V, glucose uptake with [^{18}F]FDG (2-deoxy-2-[^{18}F]fluoro-D-glucose) positron emission tomography (PET), and cellular proliferation with [^{18}F]FLT (3'-[^{18}F]fluoro-3'-deoxythymidine)-PET. Data presented herein illustrate that molecular imaging of apoptosis can accurately predict Tz-induced regression of both MMTV/HER2 transgenic mouse mammary tumors and BT474 human breast cancer cell line xenografts and may warrant further exploration clinically. Although modest overall uptake of [^{18}F]FLT limited the predictive value of [^{18}F]FLT-PET imaging in MMTV/HER2 tumors, [^{18}F]FLT-PET accurately predicted Tz response in BT474 xenografts. In both preclinical models, Tz therapy did not appear to alter glucose uptake substantially enough to afford [^{18}F]FDG-PET predictive value within this setting.

MATERIALS AND METHODS

Animal model

The MMTV/HER2 transgenic mouse line, which expresses a transgene encoding MMTV promoter-driven human HER2 (15), was a gift from Sharon Erickson (Genentech, South San Francisco, CA). MMTV/HER2 females were used to generate mammary tumors. These mice develop mammary tumors with a latency of 8–12 months. Tumors were harvested, divided in fragments, and transplanted subcutaneously (~2 mm pieces) near the mammary fat pad #1 of 4 to 6-week old female FVB syngeneic mice as previously described (16). When the grafted tumors grew to $\geq 200\text{mm}^3$, mice were imaged for baseline NIR700-Annexin-V uptake, [^{18}F]FDG accumulation, and [^{18}F]FLT uptake. The mice were then treated with trastuzumab (Tz, Herceptin®, Vanderbilt University Hospital Pharmacy; 35 mg/kg) or phosphate-buffered saline (PBS) vehicle twice per week by intraperitoneal (i.p.) injection (0.2 mL). For the BT474 model, athymic nude female mice (4–5 wks of age, Harlan) were implanted subcutaneously with E2 pellets (0.72 mg, 60-day release, Innovative Research of America) on the dorsal flank. The next day, mice were injected subcutaneously on the upper back with 2×10^7 BT474 cells (a gift from AstraZeneca) suspended in serum-free medium and mixed with Matrigel (BD Biosciences) at 1:1 ratio as described (17). Tumor diameters were measured before each treatment using calipers and volume in mm^3 calculated as described below. All mice were maintained in a specific pathogen– free facility in accordance with the Institutional Animal Care and Use Committee of the Vanderbilt University Medical Center.

Synthesis of NIR700-Annexin-V imaging probe

Synthesis of NIR700-Annexin-V has been reported previously (18). Briefly, Annexin-V (A9460, Sigma Aldrich, St. Louis, MO) was reconstituted in ice-cold 1× PBS (pH 7.4, 0.2 g/L). Near-infrared (NIR) dye (IRDye 700DX NHS ester, LI-COR Biosciences, Lincoln, NE), dissolved in dry dimethyl sulfoxide (DMSO) per manufacturer's specifications, was added to the Annexin-V solution with vortex mixing (dye to protein stoichiometry 9:1). The conjugation reaction vessel was protected from light and gently agitated for 2 h at room temperature. Labeling progress was monitored *via* gel filtration chromatography (Superdex 200HR, Amersham Pharmacia), eluting with 1× PBS. Following conjugation, labeled probes were purified exhaustively by dialysis (1× PBS, 4°C) using 7000 molecular weight cutoff (MWCO) Slide-A-Lyzer dialysis cassettes (Pierce of Thermo Fisher Scientific, Rockford, IL). The purity of the conjugates was assessed chromatographically and dye:protein ratio (routinely 1:1) was quantified by spectrophotometry.

Synthesis of [^{18}F]FLT

[^{18}F]FLT was prepared from [^{18}F]fluoride in a two-step, one-pot reaction as previously described (27) using a GE TRACERlab® FX-FN automated module. Aqueous [^{18}F]fluoride from an H_2[^{18}O]O target was trapped by ion exchange (QMA®, Waters, Milford, MA) and then eluted with Kryptofix-222 (K_{222}) and K_2CO_3 in CH_3CN/H_2O into the reaction vessel. Three sequences of heating (110°C) with He(*g*) flow resulted in dry [^{18}F]-fluoride/K_{222}/K_2CO_3. The cyclic precursor 2,3'-anhydro-5'-O-benzoyl-2'-deoxythymidine (ABX Advanced Biochemical Compounds, Radeberg, Germany) was added in DMSO and reacted for 10 min at 160°C. The benzoyl protecting group was removed from the labeled intermediate by basic hydrolysis (0.25 M NaOH, 50°C, 10 min). The reaction mixture was purified on a semipreparative C-18 HPLC column eluting with 10% ethanol/10 mM sodium phosphate buffer and sterilized by 0.2 micron membrane filtration. Radiochemical identity, purity and specific activity were determined by analytical HPLC. Product was obtained with average radiochemical purity of 98.3% and specific activity of 3,480 Ci/mmol.

Procurement of [^{18}F]FDG

[^{18}F]FDG was synthesized in the Vanderbilt University Medical Center Radiopharmacy and distributed by PETNET. The average radiochemical purity of the product was 98.5% and specific activity was > 1,000 Ci/mmol.

In vivo imaging

Mice were imaged with NIR700-Annexin-V, [^{18}F]FLT and [^{18}F]FDG weekly prior to and within 24 h of administration of Tz or PBS for up to three weeks or until complete tumor regression was observed. Inclusion criteria were baseline tumor size between 200–900mm^3. During the imaging sessions, the mice were kept under general anesthesia by inhalation of 1–3% isoflurane with 2% oxygen (and on a warm water pad during PET imaging).

NIR700-Annexin-V imaging—Prior to imaging, the fur was removed (MMTV/HER2 only) from the right dorsal half of the mouse using a commercial depilatory cream (Nair ®, Church & Dwight Co. Inc., Princeton, NJ) in order to reduce scatter and absorbance from overlying fur. NIR images were acquired using a Maestro FLEX *In Vivo* Imaging system (CRI®, Woburn, MA) equipped with the F-filter set (spectral range of 680–950nm, 500 ms exposure time, stage height of 1, and 2.8 f-stop). Pre-injection autofluorescence images were acquired with mice in the lateral decubitus position with the tumor facing the camera lens. The mice were then retroorbitally injected with NIR700-Annexin-V (0.5 nmol). Longitudinal images were acquired immediately after the injection and subsequently at regular intervals for up to 44 h

post-injection. Time-fluorescence activity curves were generated for each mouse at each imaging session as described below.

[^{18}F]FDG-PET and [^{18}F]FLT-PET imaging—Animal handling methods in preparation for and during [^{18}F]FDG-PET imaging were similar to published protocols (19,20). Briefly, prior to imaging, the mice were fasted overnight and were allowed to acclimate to the PET imaging facility environment for at least one h while on a warm water pad. [^{18}F]FDG and [^{18}F]FLT were administered on different days *via* a single retroorbital injection of ~200 μCi (100 μL). Following a 40-min distribution period, 20-min static PET scans were collected on a Concorde Microsystems microPET Focus 220 (Siemens). Mice were awake during the uptake period and were maintained on a warm water heating pad. PET images then were reconstructed using the ordered-subsets expectation-maximization (OSEM) algorithm.

Immunohistochemistry (IHC)

Immediately following imaging, mice were euthanized and tumor tissues were collected for IHC analysis. Tissues were fixed in 4% formalin for 24 h and subsequently transferred to 70% EtOH prior to processing and paraffin embedding. Tissues were examined by hematoxylin and eosin (H&E) staining to verify that adequate tumor tissue was present. Subsequently, tissues were immunostained using antibodies against cleaved caspase-3, S473 p-AKT (Cell Signaling,), and Ki67 (Biocare, Dako). Cleaved caspase-3 positive cells were counted from five randomly selected fields at 100× magnification and results expressed as % positive cells cells/field. Ki67 and S473 p-AKT were evaluated by an expert pathologist (M.G.O.) as described previously (21).

Data analysis

Tumor volume—Tumor volume was calculated using the following formula:

$$Volume = \frac{length \times length \times width}{2},$$

where length is the smaller dimension. Percent change in tumor volume from baseline was then calculated using the formula:

$$\%\Delta_{Volume} = \frac{Vol_{t=X} - Vol_{t=0}}{Vol_{t=0}} \times 100$$

Tz-treated tumors were defined as “responding” to therapy if the total tumor volume decreased by 20% or more from baseline by either the end of two weeks of treatment (BT474) or three weeks of treatment (MMTV/HER2).

Optical imaging analysis—Images acquired with a Maestro FLEX *In Vivo* imaging system were spectrally unmixed using CRI-supplied software version 0.9.3. Any animals exhibiting post-injection dose infiltration were excluded from imaging analysis. The average intensity of NIR700-Annexin-V in the manually-defined tumor region of interest (ROI) was quantified and compared to that in the right thigh muscle ROI, which served as an internal reference at each imaging time point for each mouse. Time versus NIR700-Annexin-V intensity plots were generated for tumor and muscle and the area under the curve (AUC) was calculated for both tumor and muscle at each imaging time point using a trapezoidal integration. The ratio of tumor AUC and muscle AUC (T/M AUC) was quantified for each imaging session and the percent change in T/M AUC from baseline was subsequently calculated using the formula:

$$\%\Delta_{T/M(AUC)} = \frac{T/M(AUC)_{t=X} - T/M(AUC)_{t=0}}{T/M(AUC)_{t=0}} \times 100$$

The T/M ratio at each imaging time point for each mouse was then plotted with respect to the number of treatments received and statistical analyses were performed using a paired t-test. The % change in the T/M AUC was also plotted relative to the % change in tumor size and fitted to a one phase exponential fit to assess the degree of correlation.

[^{18}F]FDG-and [^{18}F]FLT-PET analysis—Any animals exhibiting significant post-injection dose infiltration were excluded from imaging analysis. The maximum standard uptake values (SUVs) were quantified by manually drawing ROIs around the tumor using ASIPro VM (CTI Concorde Microsystems, Knoxville, TN) and normalizing the signal intensity to the injected dose and mouse mass. SUV_{max} was selected for PET imaging analysis to eliminate potential bias in the quantified data due to tumor heterogeneity. The percent change in SUV_{max} from baseline was subsequently calculated using the formula:

$$\%\Delta_{\max SUV} = \frac{\max SUV_{t=X} - \max SUV_{t=0}}{\max SUV_{t=0}} \times 100$$

and plotted with respect to the weeks of treatment received. For display purposes, PET images are presented on similar normal tissue activity scales. Statistical analysis was performed using a paired t-test.

RESULTS

Trastuzumab-induced regression of MMTV/HER2 and BT474 mammary tumors

Similar to our prior observations (16), a significant fraction of tumors derived from MMTV/HER2 transgenic mice responded to Tz therapy, defined as a reduction of tumor volume greater than 20% by the end of the three-week regimen. For analysis, MMTV/HER2 tumor mice were stratified as responders (16/30) or non-responders (14/30) according to the change in tumor size from baseline. Tumors that were initially responsive regressed proportionately with successive Tz treatments. In contrast, non-responding MMTV/HER2 tumors grew significantly over the course of treatment (Supplementary Figure 1A/B). We found BT474 tumors to be considerably more sensitive to Tz treatment, noting that all Tz-treated tumors, but not vehicle-treated tumors, demonstrated significant regression following two-weeks of treatment (Supplementary Figure 2A/B).

Imaging apoptosis with NIR700-Annexin-V in MMTV/HER2 model predicts tumor regression

Prior to and one week following Tz treatment, no significant accumulation of NIR700-Annexin-V was observed in MMTV/HER2 tumors. However, after two weeks of treatment, significant accumulation of NIR700-Annexin-V was observed in the tumors of responding but not non-responding mice (Figure 1). Immediately following injection of NIR700-Annexin-V, renal accumulation was noted in all mice (Figure 1). Clearance profile analysis was performed longitudinally on each mouse to assess the relative accumulation of NIR700-Annexin-V in tumors and in reference muscle tissue (Supplementary Figure 3). From this analysis, tumor probe accumulation was significantly increased after two weeks of treatment and thereafter compared to baseline in responding mice (Figure 2A, ($p<0.0005$). The mean NIR700-Annexin-V tumor uptake (T/M AUC ratio) in responding tumors increased by 9.7%, 46%, and 69% after one, two, and three weeks of Tz treatment, respectively. In contrast, NIR700-Annexin-V did

not accumulate in MMTV/HER2 tumors that did not shrink with treatment (Figure 2B). Interestingly, we noted increased NIR700-Annexin-V accumulation in tumors after two weeks of therapy in all but one MMTV/HER2 responder (Figure 2C), yet we actually noted decreased accumulation of the imaging probe over the same timeframe in non-responders of the same model (Figure 2D). Importantly, analysis of all MMTV/HER2 imaging data from responder and non-responder mice over the entire three-week treatment course indicated that the magnitude of NIR700-Annexin-V uptake in tumors was inversely proportional to the change in tumor size from baseline (Figure 2E). Non-linear regression analysis of all NIR700-Annexin-V imaging data points demonstrated a significant negative correlation between change in tumor size and NIR700-Annexin-V tumor uptake ($R^2 = 0.375$). Thus, tumors exhibiting increased accumulation of NIR700-Annexin-V regressed, while tumors with reduced NIR700-Annexin-V accumulation progressed on therapy.

Trastuzumab does not alter tumor [^{18}F]FDG uptake in MMTV/HER2 model

Prior to Tz treatment, MMTV/HER2 tumors of responding and non-responding mice were differentiable from background by PET imaging of [^{18}F]FDG uptake (Figure 3A/B). However, throughout the 3-week treatment course, no statistically significant difference was observed between baseline [^{18}F]FDG uptake and uptake following successive Tz treatments in responding or non-responding mice (Figure 4A/B). Over the first 2 weeks of therapy, the majority of responding mice (71%) showed similar [^{18}F]FDG uptake post-Tz treatment when compared to baseline (Figure 4C), suggesting that [^{18}F]FDG uptake is not a suitable predictive biomarker in this setting. Although tumor [^{18}F]FDG uptake in non-responding mice appeared to trend upward when comparing baseline and two-week images (Figure 4D), the trend was non-significant. Furthermore, in the overall population of treated and untreated MMTV/HER2 tumor-bearing mice, no correlation was observed between tumor size and [^{18}F]FDG uptake (Figure 4E).

MMTV/HER2 tumors exhibit poor [^{18}F]FLT uptake

Only modest tumor uptake of [^{18}F]FLT was observed prior to Tz treatment in both responding and non-responding MMTV/HER2-bearing cohorts. (Supplementary Figure 5A). Subsequent treatment with Tz had no discernable affect on tumor uptake of [^{18}F]FLT (Supplementary Figure 5B) through two weeks of treatment, over which time many responding tumors exhibited significant regression. Ki67 immunoreactivity of tumor tissues collected from treated mice demonstrated a modest increase compared to the tumors of untreated mice (Figure 5). As a result, [^{18}F]FLT-PET imaging was discontinued in MMTV/HER2 tumor-bearing after the second week of treatment and not considered further in this model.

Trastuzumab-induced tumor regression correlates with increased apoptosis in MMTV/HER2 tumors

MMTV/HER2 tumor tissues were evaluated for cleaved caspase-3, Ki67, and phospho-AKT (p-AKT) immunoreactivity. Responding MMTV/HER2 tumors collected after three weeks of treatment exhibited significantly increased cleaved caspase-3 immunoreactivity compared to untreated or non-responding cohorts (Figure 5). Furthermore, MMTV/HER2 tumor tissues that were collected before or subsequent to each week of Tz treatment revealed a proportionately increased number of apoptotic cells over time on treatment (Supplementary Figure 4), in agreement with NIR700-Annexin-V imaging. On average in responding MMTV/HER2 tumors, 0.69%, 1.1%, and 1.3% caspase-3+ cells were detected per tumor field following one, two, and three weeks of Tz treatment respectively ($p < 0.05$), compared to 0.24% detected at baseline. Although MMTV/HER2 tumors appeared proliferative, we did not observe a consistent correlation between % Ki67-immunoreactive cells and Tz treatment or response in this model. We also observed variability in p-AKT immunoreactivity between all MMTV/

HER2 tumors, and thus did not find a correlation between p-AKT and response. These results appear to be consistent with tumor [^{18}F]FDG uptake in this model which was also variable.

Apoptosis imaging and [^{18}F]-FLT PET imaging predict response to Tz in BT474 xenografts

All Tz-treated BT474 tumor-bearing mice carried out as far as two-weeks of therapy exhibited significant tumor regression (Supplementary Figure 2). We therefore evaluated the potentially predictive imaging metrics following just one week of Tz treatment in this model. Similar to our observations in responding MMTV/HER2 tumor-bearing mice, we found that NIR700-Annexin-V accumulation was predictive of response to treatment. In BT474 tumor bearing mice, the difference between NIR700-Annexin-V accumulation in vehicle-treated and Tz-treated tumors was statistically significant following just a single week of therapy (Figure 6A–6D). Also similar to the MMTV/HER2 studies, Tz-treatment did not appear to have any observable affect on [^{18}F]FDG uptake in BT474 tumors (Figure 6E–H). We found that baseline [^{18}F]FLT uptake in BT474 tumors was considerably higher compared to MMTV/HER2 tumors. Additionally, one week of Tz-treatment significantly reduced [^{18}F]FLT uptake in this model (Figure 6I–L). In similar fashion to the MMTV/HER2 studies, we found good agreement between each of the imaging metrics and histology (Supplementary Figures 6 and 7), where we noted significantly elevated caspase 3 staining and significantly decreased Ki67 staining in Tz-treated BT474 tumors following both one and two weeks of therapy. As with MMTV/HER2 tumors, Tz-treatment did not appear to significantly affect pAKT staining in BT474 tumor tissues.

DISCUSSION

In contrast with predominantly anatomical imaging modalities such as computed tomography (CT), planar x-ray, or magnetic resonance imaging (MRI), non-invasive molecular imaging aims to visualize and quantify cellular and physiological processes *in vivo*. Since specific biological changes may occur in tumors within hours to days of treatment and therefore precede clinical regression, imaging biomarkers capable of assessing the most relevant of these molecular events may be highly suitable for detecting early responses and potentially predicting treatment outcome. Validation of such imaging metrics forms the basis of important research occurring at the interface between imaging science and cancer biology.

Clinically, the PET tracer [^{18}F]FDG is recognized as a tool for cancer detection and staging in most organ sites. In addition to [^{18}F]FDG, additional tracers such as [^{18}F]FLT-PET to assess proliferation, as well as Annexin-V conjugates to assess apoptosis, offer great promise as a means to evaluate response to conventional and molecularly-targeted therapeutic interventions (22–24). Selection criteria for appropriate molecular imaging biomarker(s) is highly dependent upon the underlying tumor cell biology and its modulation following therapeutic intervention. For example, capitalizing upon the role that EGFR serves in mediating tumor cell proliferation and apoptosis, we recently illustrated that molecular imaging assessments of these events are potentially biomarkers of response to EGFR-directed therapy in colorectal cancer (CRC) (25).

In this study, we have evaluated three independent molecular imaging metrics as potential biomarkers of response to the HER2 antibody Tz in a mouse model of HER2+ breast cancer. Each imaging metric was selected to report a type of cellular response and was evaluated within the context of responding and non-responding tumor-bearing cohorts. Data presented here illustrate that accumulation of an Annexin-V-based optical imaging probe in Tz-treated, MMTV/HER2 transgenic mouse tumor allografts, as well as in BT474 human xenografts, correlates with response and predicts clinical regression before evident by physical means. In the more responsive BT474 model, [^{18}F]FLT-PET also appeared to be a potential biomarker of response to Tz. The variability we noted in tumor [^{18}F]FLT uptake when comparing these

two preclinical models studied likely has biological significance. Theoretically, [^{18}F]FLT and other nucleoside-based tracers serve as a surrogate markers of proliferation by reporting the activity of the thymidine salvage pathway, a cellular mechanism that utilizes uptake of deoxyribonucleosides from the extracellular environment to provide dividing cells with DNA precursors. However, thymidine salvage is not a prerequisite for cell survival in replicating mammalian cells. In fact, thymidine salvage is a complementary route for providing cells with nucleosides and *de novo* synthesis of nucleosides is fully capable of providing all the DNA precursors that are needed for cell growth (13). Thus, [^{18}F]FLT uptake (if observed) in tumors relying predominately or completely on *de novo* nucleoside synthesis may poorly inform proliferation status compared with tumors that rely more heavily on thymidine salvage. Although beyond the scope of these studies, this could explain differences in [^{18}F]FLT uptake between MMTV/HER2 and BT474 tumors. At present time, the prognostic and therapeutic implications for tumors that utilize *de novo* nucleoside synthesis versus thymidine salvage are not well understood and additional research within this area should be conducted.

In both MMTV/HER2 and BT474 tumors, [^{18}F]FDG showed significant uptake ($\geq 2\times$ background), but this was unchanged in response to Tz treatment. This finding is significant because recent human studies have shown higher [^{18}F]FDG uptake in triple-negative compared to hormone receptor-positive breast cancers (26). Furthermore, human studies have suggested that adequate measures of treatment response with [^{18}F]FDG PET imaging are more difficult in tumors exhibiting modest pre-treatment uptake of [^{18}F]FDG (27).

Importantly, trends observed between imaging metrics and standard histological markers (namely cleaved caspase-3, activated AKT (p-AKT), and Ki67) exhibited temporal agreement, suggesting that the observations made by imaging were reflective of molecular and cellular events in tumors *in situ*. Cleaved caspase-3 immunoreactivity was directly proportional to, and temporally correlated with, NIR700-Annexin-V tumor uptake and response to Tz treatment in both MMTV/HER2 and BT474 tumors. In the analysis of p-AKT staining of MMTV/HER2 tumor tissues, a portion of the cells collected from the tumors of treated, responding mice demonstrated decreased p-AKT, while other cells showed significantly increased cytoplasmic p-AKT. Thus, we did not observe a consistent net difference in p-AKT staining across treated, untreated, responding, and non-responding cohorts in this model. Similarly, we did not observe differential p-AKT staining across Tz-or vehicle-treated BT474 tumors. Although numerous biological factors affect glucose metabolism, the lack of sensitivity observed with [^{18}F]FDG-PET imaging in these studies appears consistent with the lack of modulation of p-AKT (12). In agreement with previous clinical findings that showed no correlation between Ki67 immunoreactivity and response to neoadjuvant Tz in patients with HER2+ locally advanced breast cancer (11), neither Ki67 immunoreactivity or [^{18}F]FLT-PET were reflective of response to Tz in the MMTV/HER2 model. These results mirror our recent findings in the evaluation of [^{18}F]FLT-PET imaging as a biomarker of response to the EGFR therapeutic antibody cetuximab (mAb-C225) in human colorectal cancer (CRC) xenografts. In these studies, we noted excellent correlation between [^{18}F]FLT-PET imaging and tumor Ki67 immunoreactivity, yet similarly to the Tz results, cetuximab was ineffective at reducing tumor cell proliferation *in vivo* (18). In contrast, Tz treatment was effective at reducing proliferation in the more responsive BT474 tumors as assessed by Ki67 immunoreactivity., This effect was predictable with [^{18}F]FLT-PET imaging following just 1 week of therapy.

In conclusion, molecular imaging of apoptosis appears to be a promising noninvasive method for prediction and evaluation of early response to Tz therapy. Although the Annexin-V analogue reported here employed an optical imaging label and may be best suited for preclinical imaging, our data suggest that pharmacodynamic clinical evaluation of apoptosis in real time in breast cancer patients is warranted and feasible via functionalization with ^{99m}Tc for SPECT imaging (28). Data presented in these studies also suggest that [^{18}F]FLT-PET imaging is

potentially an informative biomarker in this setting, especially for some exquisitely sensitive tumors. However, the discrepancy observed between baseline uptake of [^{18}F]FLT across the MMTV/HER2 and BT474 preclinical models indicates that additional studies are needed to further elucidate the biological basis of FLT-PET imaging as a biomarker in breast cancer. While single agent trastuzumab did not consistently alter glucose metabolism substantially enough to afford [^{18}F]FDG-PET predictive value in these studies, this metric remains potentially appropriate for use in evaluating other novel, molecularly-targeted regimens in breast cancer that may include Tz combined with other novel therapies.

Statement of Translational Relevance

The development of inhibitors targeting various portions of the ErbB signaling axis is an active and clinically important area of research. Trastuzumab (Tz, Herceptin®) is an FDA-approved, recombinant, humanized monoclonal antibody that selectively binds to the extracellular domain of HER2. Objective means to assess early response to Tz therapy remain undeveloped. To this end, we have evaluated three translational, noninvasive molecular imaging metrics to quantify and predict response to Tz in preclinical mouse models of HER2-overexpressing breast cancer.

Supplementary Material

Refer to Web version on PubMed Central for supplementary material.

Acknowledgments

Funding: This work was supported by pilot funding from the NCI SPORE in Breast Cancer 5P50 CA098131, R01 CA80195, and the South-Eastern Center for Small-Animal Imaging (U24 CA126588). HCM is supported by a Career Development Award from the NCI (K25 CA127349). TWM is supported by NCI grant F32 CA121900. SKW and ETM are supported by training grants in imaging science (T32 EB003817 and T32 EB03817). JRB is supported by a training grant in cancer imaging (5R25 CA092043-08). CS is supported by a research fellowship funded by the department of Radiology and Radiological Sciences.

REFERENCES

1. American Cancer Society. Cancer Facts & Figures 2008. Atlanta: American Cancer Society; 2008.
2. Slamon DJ, Clark GM, Wong SG, Levin WJ, Ullrich A, McGuire WL. Human breast cancer: correlation of relapse and survival with amplification of the HER-2/neu oncogene. Science 1987;235:177–182. [PubMed: 3798106]
3. Slamon DJ, Godolphin W, Jones LA, et al. Studies of the HER-2/neu proto-oncogene in human breast and ovarian cancer. Science 1989;244:707–712. [PubMed: 2470152]
4. Harari D, Yarden Y. Molecular mechanisms underlying ErbB2/HER2 action in breast cancer. Oncogene 2000;19:6102–6114. [PubMed: 11156523]
5. Carter P, Presta L, Gorman CM, et al. Humanization of an anti-p185HER2 antibody for human cancer therapy. Proceedings of the National Academy of Sciences of the United States of America 1992;89:4285–4289. [PubMed: 1350088]
6. Baselga J, Tripathy D, Mendelsohn J, et al. Phase II study of weekly intravenous recombinant humanized anti-p185HER2 monoclonal antibody in patients with HER2/neu-overexpressing metastatic breast cancer. J Clin Oncol 1996;14:737–744. [PubMed: 8622019]
7. Cobleigh MA, Vogel CL, Tripathy D, et al. Multinational study of the efficacy and safety of humanized anti-HER2 monoclonal antibody in women who have HER2-overexpressing metastatic breast cancer that has progressed after chemotherapy for metastatic disease. J Clin Oncol 1999;17:2639–2648. [PubMed: 10561337]
8. Vogel CL, Cobleigh MA, Tripathy D, et al. Efficacy and safety of trastuzumab as a single agent in first-line treatment of HER2-overexpressing metastatic breast cancer. J Clin Oncol 2002;20:719–726. [PubMed: 11821453]

9. Slamon DJ, Leyland-Jones B, Shak S, et al. Use of chemotherapy plus a monoclonal antibody against HER2 for metastatic breast cancer that overexpresses HER2. N Engl J Med 2001;344:783–792. [PubMed: 11248153]
10. Valabrega G, Montemurro F, Aglietta M. Trastuzumab: mechanism of action, resistance and future perspectives in HER2-overexpressing breast cancer. Ann Oncol 2007;18:977–984. [PubMed: 17229773]
11. Mohsin SK, Weiss HL, Gutierrez MC, et al. Neoadjuvant trastuzumab induces apoptosis in primary breast cancers. J Clin Oncol 2005;23:2460–2468. [PubMed: 15710948]
12. Plas DR, Thompson CB. Akt-dependent transformation: there is more to growth than just surviving. Oncogene 2005;24:7435–7442. [PubMed: 16288290]
13. Majumder PK, Febbo PG, Bikoff R, et al. mTOR inhibition reverses Akt-dependent prostate intraepithelial neoplasia through regulation of apoptotic and HIF-1-dependent pathways. Nature medicine 2004;10:594–601.
14. Yakes FM, Chinratanalab W, Ritter CA, King W, Seelig S, Arteaga CL. Herceptin-induced inhibition of phosphatidylinositol-3 kinase and Akt Is required for antibodymediated effects on p27, cyclin D1, and antitumor action. Cancer Res 2002;62:4132–4141. [PubMed: 12124352]
15. Finkle D, Quan ZR, Asghari V, et al. HER2-targeted therapy reduces incidence and progression of midlife mammary tumors in female murine mammary tumor virus huHER2-transgenic mice. Clin Cancer Res 2004;10:2499–2511. [PubMed: 15073130]
16. Reyzer ML, Caldwell RL, Dugger TC, et al. Early changes in protein expression detected by mass spectrometry predict tumor response to molecular therapeutics. Cancer research 2004;64:9093–9100. [PubMed: 15604278]
17. Arpino G, Gutierrez C, Weiss H, et al. Treatment of human epidermal growth factor receptor 2-overexpressing breast cancer xenografts with multiagent HER-targeted therapy. J Natl Cancer Inst 2007;99:694–705. [PubMed: 17470737]
18. Manning NBM, HCharles; Foutch, ACoe; Virostko, JohnM; Wyatt, ShelbyK; Shah, Chirayu; McKinley, EliotT; Xie, Jingping; Mutic, NathanJ; Washington, MKay; Lafleur, Bonnie; Tantawy, MohammedNoor; Peterson, ToddE; Ansari, MSib; Baldwin, RonaldM; Rothenberg, MaceL; Bornhop, DarrylJ; Gore, JohnC; Coffey, RobertJ. Molecular imaging of therapeutic response to EGF receptor blockade in colorectal cancer. Clinical Cancer Research. 2008 in press.
19. Fueger BJ, Czernin J, Hildebrandt I, et al. Impact of animal handling on the results of 18F-FDG PET studies in mice. J Nucl Med 2006;47:999–1006. [PubMed: 16741310]
20. Dandekar M, Tseng JR, Gambhir SS. Reproducibility of 18F-FDG microPET studies in mouse tumor xenografts. J Nucl Med 2007;48:602–607. [PubMed: 17401098]
21. Guix M, Granja Nde M, Meszoely I, et al. Short preoperative treatment with erlotinib inhibits tumor cell proliferation in hormone receptor-positive breast cancers. J Clin Oncol 2008;26:897–906. [PubMed: 18180460]
22. Czernin J, Weber WA, Herschman HR. Molecular imaging in the development of cancer therapeutics. Annual Review of Medicine 2006;57:99–118.
23. DeNardo SJ. Combined molecular targeting for cancer therapy: A new paradigm in need of molecular imaging. Journal of Nuclear Medicine 2006;47:4–5. [PubMed: 16391180]
24. Rudin M, Weissleder R. Molecular imaging in drug discovery and development. Nature Reviews Drug Discovery 2003;2:123–131.
25. Manning HC, Merchant NB, Foutch AC, et al. Molecular imaging of therapeutic response to epidermal growth factor receptor blockade in colorectal cancer. Clin Cancer Res 2008;14:7413–7422. [PubMed: 19010858]
26. Basu S, Chen W, Tchou J, et al. Comparison of triple-negative and estrogen receptor-positive/progesterone receptor-positive/HER2-negative breast carcinoma using quantitative fluorine-18 fluorodeoxyglucose/positron emission tomography imaging parameters: a potentially useful method for disease characterization. Cancer 2008;112:995–1000. [PubMed: 18098228]
27. McDermott GM, Welch A, Staff RT, et al. Monitoring primary breast cancer throughout chemotherapy using FDG-PET. Breast cancer research and treatment 2007;102:75–84. [PubMed: 16897427]

28. Blankenberg FG, Vanderheyden JL, Strauss HW, Tait JF. Radiolabeling of HYNIC-annexin V with technetium-99m for in vivo imaging of apoptosis. Nature protocols 2006;1:108–110.

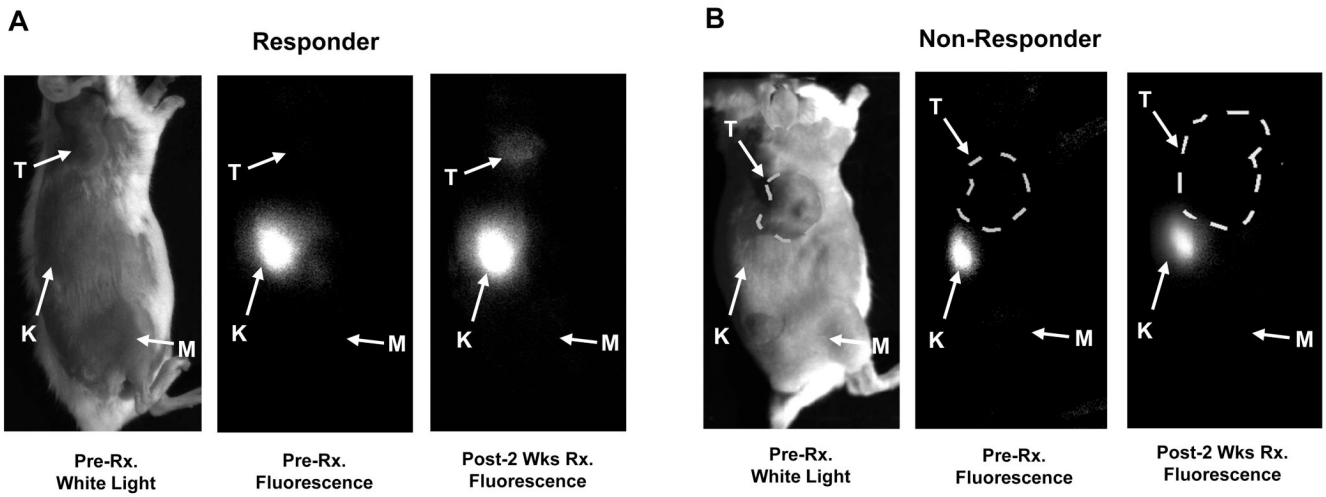

Figure 1. Accumulation of NIR700-Annexin-V is enhanced in MMTV/HER2 tumors responding to trastuzumab

NIR700-Annexin-V was administered i.v., and mice were serially imaged up to 44 h before and after treatments with Tz or vehicle (PBS). Representative images from responding (A) and non-responding (B) MMTV/HER2 tumor bearing mice (24 h images shown). Significant accumulation of NIR700-Annexin-V was observed within the responsive tumor after two weeks of Tz treatment (A), while the non-responsive tumor does not show significant NIR700-Annexin-V uptake (B). T = tumor, K = kidney, M = reference muscle.

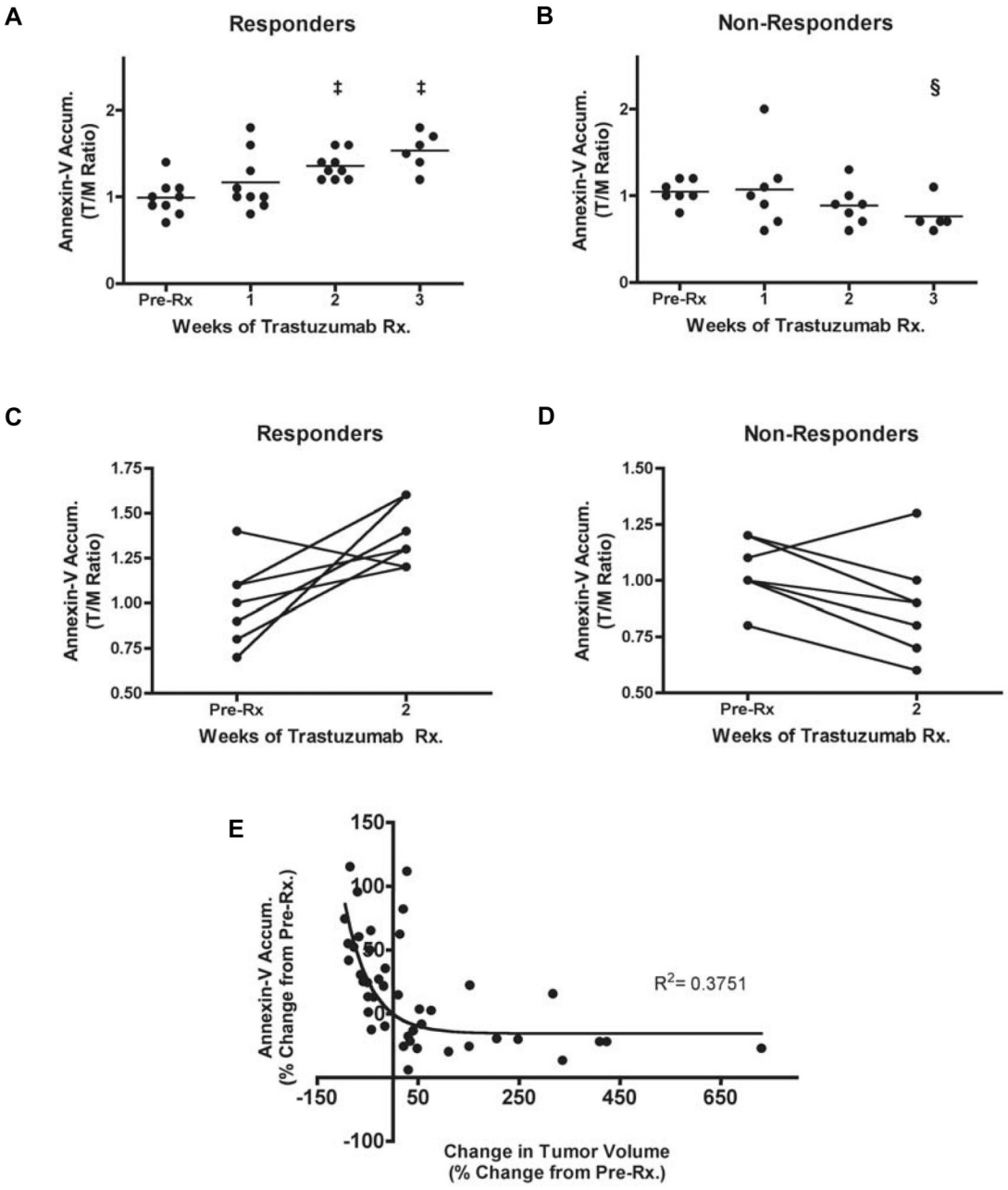

Figure 2. Longitudinal assessment of NIR700-Annexin-V accumulation in MMTV/HER2 tumors illustrates the efficacy of Tz treatment

(A) NIR700-Annexin-V accumulation ratios (T/M, tumor/normal muscle) increased and attained statistical significance following two weeks of Tz treatment in responding MMTV/HER2 tumor-bearing mice (‡ $p < 0.001$, paired t-test). (B) NIR700-Annexin-V did not accumulate in non-responding tumors, and overall uptake of the imaging probe decreased as tumors progress (§, $p < 0.05$). On an individual basis, NIR700-Annexin-V uptake (pre-Rx imaging compared to two-week post-Rx) significantly increased following treatment in the vast majority of responding MMTV/HER2 tumor-bearing mice (C). However, non-responding cohorts typically showed decreased NIR700-Annexin-V accumulation after two weeks of Tz treatment (D). (E) The magnitude of tumor regression was proportional to degree of uptake of

NIR700-Annexin-V. A non-linear inverse correlation was observed between the change in NIR700-Annexin-V uptake from baseline compared to change in tumor volume from baseline when considering all imaging time points and all mice.

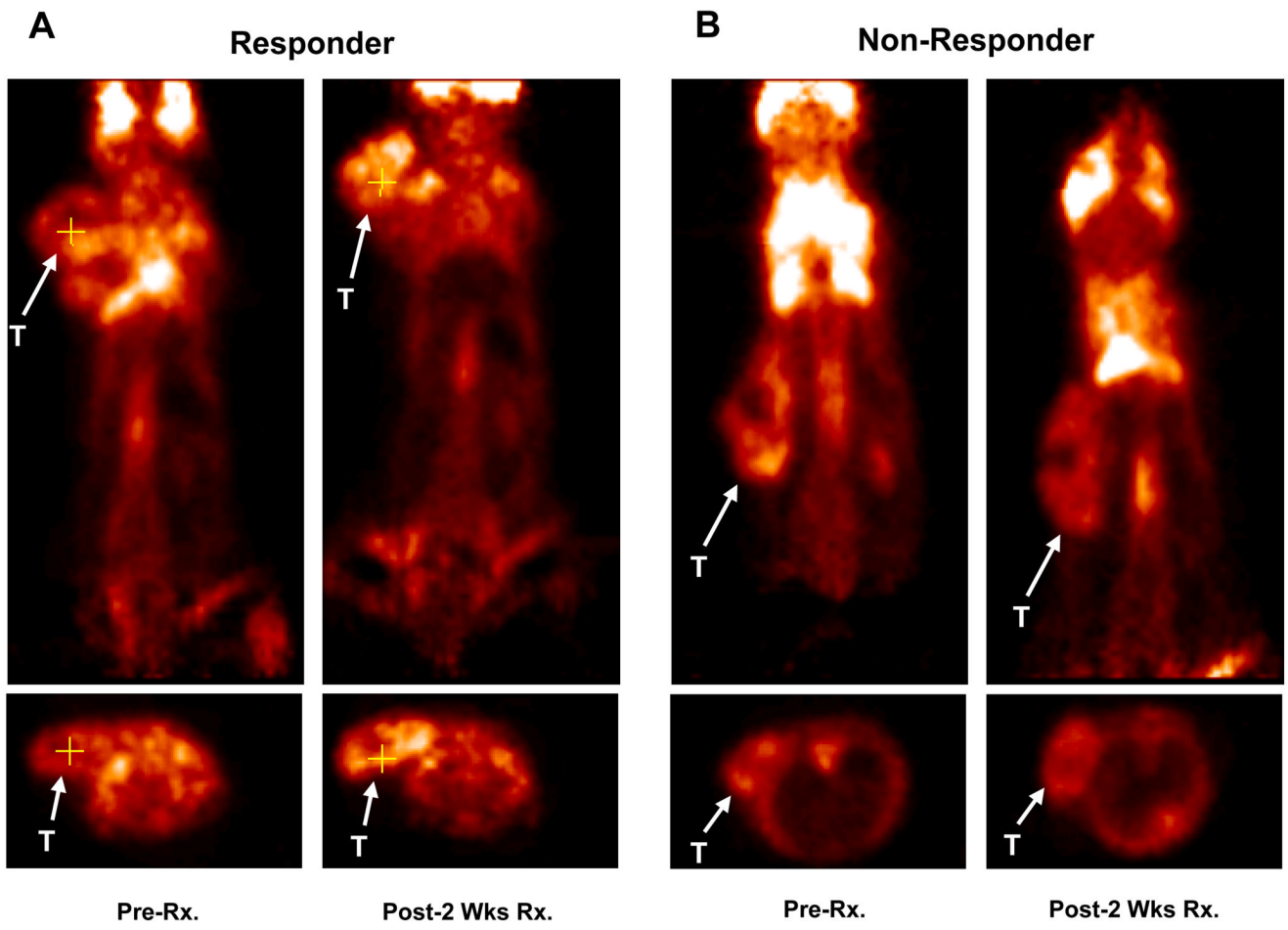

Figure 3. MMTV/HER2 tumor uptake of [^{18}F]FDG is similar across responding and non-responding cohorts

Representative [^{18}F]FDG-PET images collected prior to and following two weeks of Tz therapy in responding (A) and non-responding (B) mice. T = tumor.

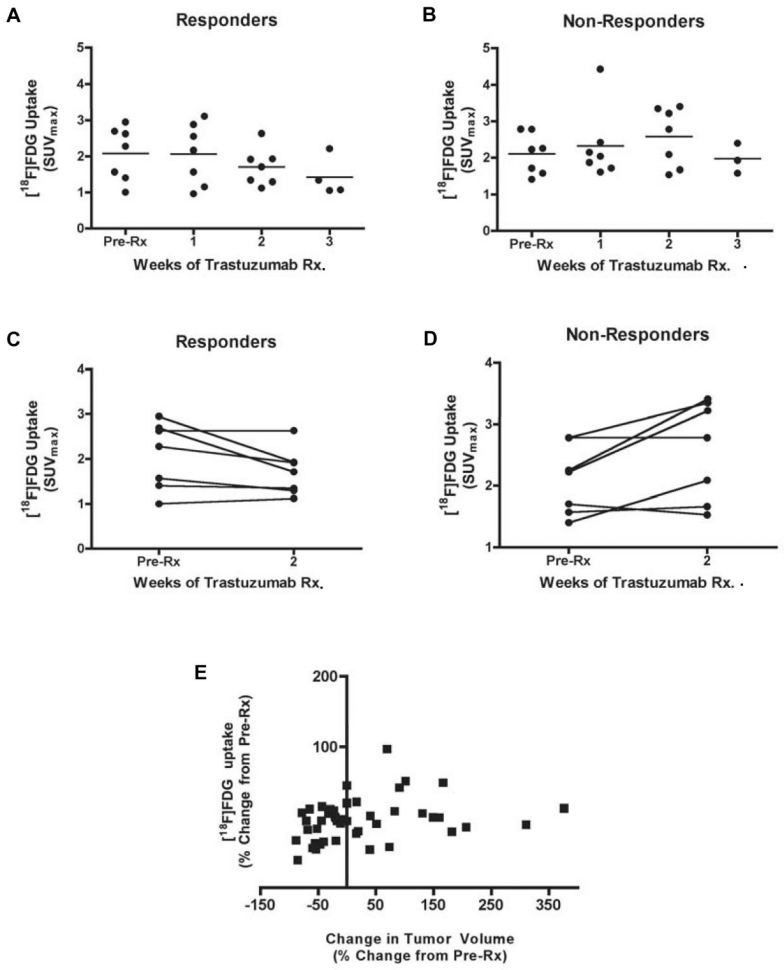

Figure 4. Longitudinal assessment of [^{18}F]FDG uptake in MMTV/HER2 tumors suggests that overall tumor glucose metabolism is not altered by Tz therapy

No significant difference was observed between serial [^{18}F]FDG-PET images in either responding (A) or non-responding (B) MMTV/HER2 tumor-bearing mice. On an individual basis, tumor [^{18}F]FDG uptake (pre-Rx imaging compared to two-week post-Rx) was almost identical following treatment in a vast majority of responding mice (C). However, some non-responding cohorts showed a trend towards increased [^{18}F]FDG uptake after two weeks of Tz (D). (E) Non-linear regression analysis demonstrated that no correlation was observed between changes in [^{18}F]FDG uptake and overall changes in tumor volume from baseline.

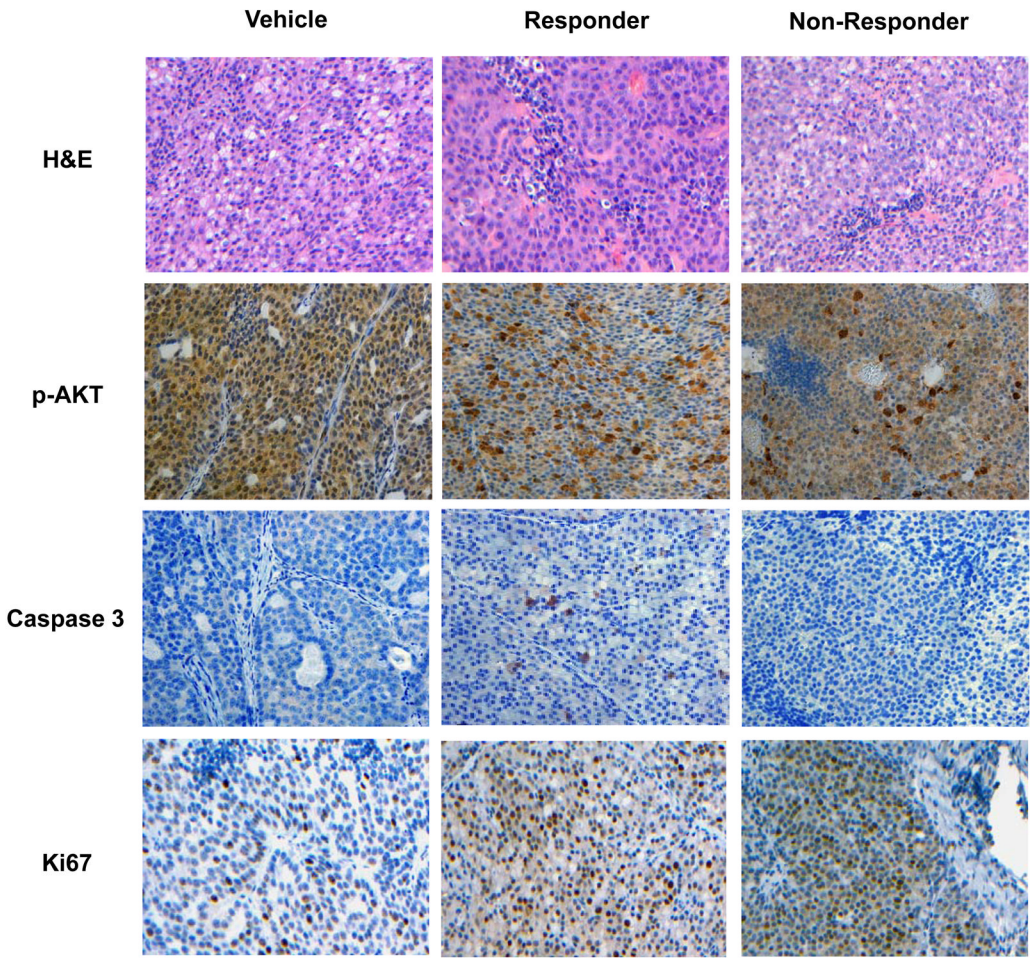

Figure 5. ***In situ*** **markers of drug action correlate with non-invasive imaging biomarkers in MMTV/HER2 tumors**

Representative tumor sections from formalin-fixed, paraffin-embedded transgenic tumor transplants stained with H&E and p-AKT, cleaved caspase-3, and Ki67 antibodies as described in Methods. Compared to vehicle treated controls, elevated cleaved caspase-3 staining was observed in MMTV/HER2 tumor tissues collected from responding, but not non-responding mice. Nuclear and cytoplasmic p-AKT immunoreactivity was observed in vehicle-treated control. Tumor tissues collected from responding mice showed a trend towards decreased nuclear p-AKT immunoreactivity, but staining was elevated significantly in the cytoplasm of many tumor cells. Similarly, non-responding cohorts demonstrated elevated cytoplasmic p-AKT, but also nuclear p-AKT that was similar to vehicle-treated cohorts. Ki67 immunoreactivity of tumor tissues was elevated following treatment with Tz compared to vehicle-treated controls.

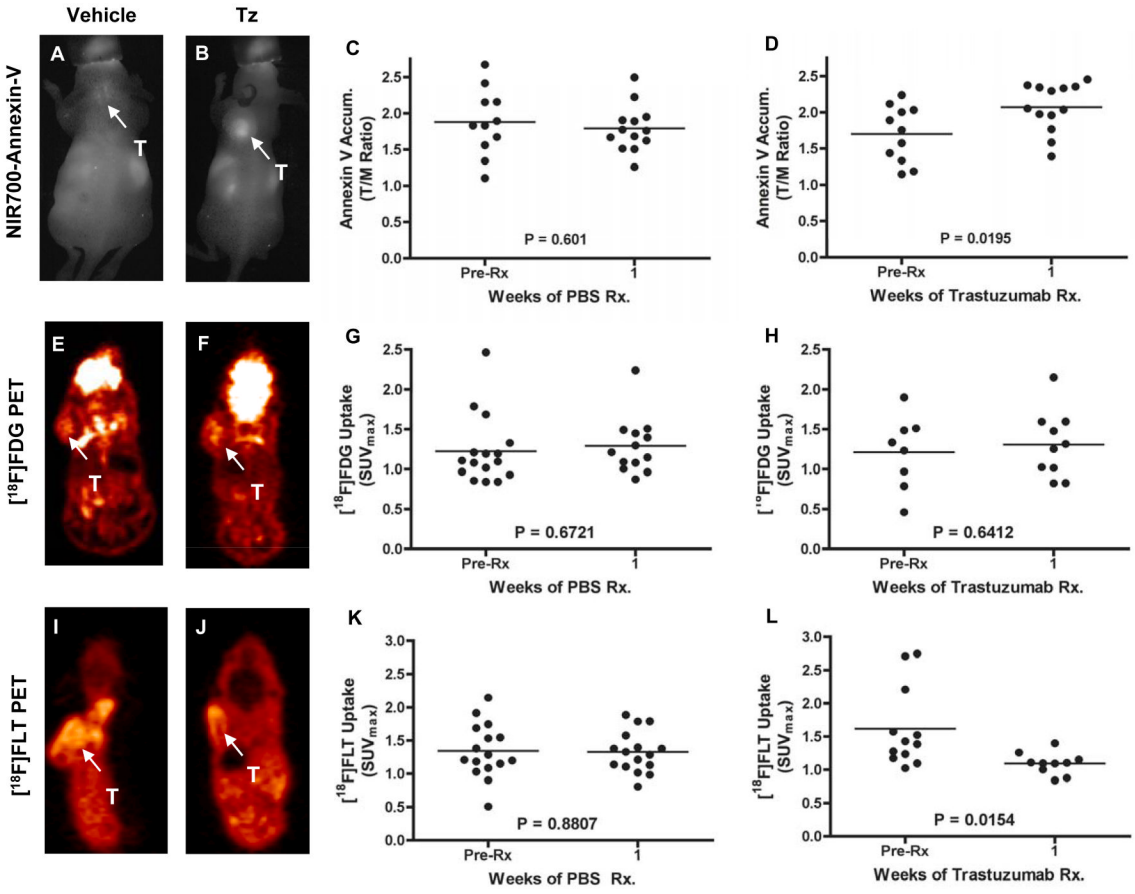

Figure 6. Longitudinal assessment of NIR700-Annexin-V accumulation, [^{18}F]FDG uptake, and [^{18}F]FLT uptake in vehicle and Tz-treated BT474 human breast cancer xenografts

NIR700-Annexin-V accumulated significantly in Tz-treated but not vehicle-treated BT474 xenografts. Representative fluorescence images of vehicle-treated (A) and Tz-treated (B) BT474 tumor-bearing mice illustrating significant accumulation of NIR700-Annexin-V in the tumor (T) of a Tz-treated mouse after 1 wk. Unlike the vehicle-treated cohort (C), statistically significant uptake of NIR700-Annexin-V was observed across a cohort of Tz-treated implicit mice (D). Similar [^{18}F]FDG uptake was observed across vehicle-treated and Tz-treated mice. Representative [^{18}F]FDG-PET images and quantified [^{18}F]FDG uptake of vehicle-treated (E/G) and Tz-treated (F/H) mice are shown. [^{18}F]-FLT accumulated significantly in BT474 xenografts of vehicle-treated mice but was significantly reduced in xenografts in Tz-treated mice. Representative [^{18}F]FLT-PET images of vehicle-treated (I) and Tz-treated (J) BT474 tumor-bearing mice illustrating significantly reduced [^{18}F]FLT uptake in the tumor (T) of a Tz-treated mouse. No change in BT474 tumor [^{18}F]FLT uptake was observed following vehicle treatment (K), yet a statistically significant decrease was observed across a cohort of Tz-treated mice (L). All images and data shown were collected after 1 week of vehicle or Tz therapy.